Pattern formation in skyrmionic materials with anisotropic environments

Julian Hagemeister, Elena y Vedmedenko, Roland Wiesendanger

▶ **To cite this version:**

Julian Hagemeister, Elena y Vedmedenko, Roland Wiesendanger. Pattern formation in skyrmionic materials with anisotropic environments. Physical Review B: Condensed Matter and Materials Physics (1998-2015), 2016, 94, pp.104434 - 104434. 10.1103/PhysRevB.94.104434 . hal-01527311

HAL Id: hal-01527311
https://hal.science/hal-01527311

Submitted on 24 May 2017

HAL is a multi-disciplinary open access archive for the deposit and dissemination of scientific research documents, whether they are published or not. The documents may come from teaching and research institutions in France or abroad, or from public or private research centers.

L'archive ouverte pluridisciplinaire **HAL**, est destinée au dépôt et à la diffusion de documents scientifiques de niveau recherche, publiés ou non, émanant des établissements d'enseignement et de recherche français ou étrangers, des laboratoires publics ou privés.

Pattern formation in skyrmionic materials with anisotropic environments

Julian Hagemeister,* Elena Y. Vedmedenko, and Roland Wiesendanger
Department of Physics, University of Hamburg, D-20355 Hamburg, Germany
(Received 1 March 2016; revised manuscript received 1 August 2016; published 28 September 2016)

Magnetic Skyrmions have attracted broad attention during recent years because they are regarded as promising candidates as bits of information in novel data storage devices. A broad range of theoretical and experimental investigations have been conducted with the consideration of axisymmetric Skyrmions in isotropic environments. However, one naturally observes a huge variety of anisotropic behavior in many experimentally relevant materials. In the present work, we investigate the influence of anisotropic environments onto the formation and behavior of the noncollinear spin states of skyrmionic materials by means of Monte Carlo calculations. We find skyrmionic textures which are far from having an axisymmetric shape. Furthermore, we show the possibility to employ periodic modulations of the environment to create skyrmionic tracks.

DOI: 10.1103/PhysRevB.94.104434

I. INTRODUCTION

Magnetic Skyrmions were originally proposed and investigated in theoretical studies [1,2], and recently they were found experimentally in the bulk and thin films of noncentrosymmetric materials [3–9] as well as in ultrathin magnetic films at crystal surfaces [10–12]. They are particlelike objects with a nonvanishing topological charge that is considered to protect them from continuous transformation into the saturated magnetic state. Together with their small lateral size in the nanometer range, this makes Skyrmions an interesting candidate for bits of information and information carriers in novel data storage devices [13,14]. Typically, magnetic Skyrmions form due to the competition of the Dzyaloshinskii-Moriya (DM) interaction [15,16] and the exchange interaction in the presence of an external magnetic field. However, the magnetic anisotropy energy may enhance the stability of magnetic Skyrmions and thus substitute an external magnetic field [5,17,18]. The DM interaction can provide a nonvanishing contribution in the presence of inversion asymmetry combined with a large spin-orbit interaction. The properties of Skyrmions have both theoretically and experimentally mainly been investigated in the context of materials providing an isotropic environment until now, which leads to the formation of Skyrmions with an axisymmetric equilibrium shape. There are only a few studies that deal with the influence of anisotropic environments, and only recently, experimental observation of Skyrmions which are deformed with respect to the axisymmetric shape has been reported for chiral magnets with crystal lattice strain [19].

However, various experimentally feasible materials naturally exhibit anisotropic behavior for multiple reasons [20–23]. In the discussion of the origins, we focus on the material systems that allow for interface-induced skyrmionic states, only. These material systems typically consist of a single or multiple atomic, magnetic layers of different atomic species which are deposited successively onto a nonmagnetic supporting crystal [24–27]. In principle, hexagonal lattices provide an isotropic environment, but the combination of materials with different lattice constants can give rise to lattice strain and reconstructions in the magnetic surface layers which then exhibit anisotropic environments, as has been discussed only recently for the double [28] and triple [29] atomic layers of Fe on Ir(111). Therefore, the influence of anisotropic environments onto the behavior of skyrmionic states is already interesting for practical reasons. More intriguing is, especially with respect to technological applications, to study the capability of tailoring the properties of Skyrmions, such as their shape and lateral position, by anisotropic environments. In particular, it is desirable to align Skyrmions on tracks along which they may be moved by means of a driving mechanism, such as, e.g., a spin-polarized electric current [14,30–32].

Here we report on Monte Carlo investigations of the magnetic pattern formation in systems with modulated environments and show skyrmionic states which exhibit shapes very different from the axisymmetric ones that have been discussed in previous studies. Also, we discuss the possibility to align Skyrmions along tracks and relate it to recent investigations conducted on the double and triple layers of Fe on Ir(111) [28,29].

We describe a skyrmionic ultrathin magnetic film by the standard effective Hamiltonian

$$H = -\sum_{\langle i,j\rangle} J_{ij}\mathbf{S}_i \cdot \mathbf{S}_j - \sum_{\langle i,j\rangle} \mathbf{D}_{ij} \cdot (\mathbf{S}_i \times \mathbf{S}_j) - \sum_i K_i \left(\mathbf{e}_{K_i} \cdot \mathbf{S}_i\right)^2 - \mu \sum_i \mathbf{B} \cdot \mathbf{S}_i, \quad (1)$$

consisting of the exchange energy, the DM energy, the magnetocrystalline anisotropy, and the Zeeman energy. The dipolar interaction is neglected because it is expected to be comparably small for thin magnetic films [33]. The classical three-dimensional spins $\mathbf{S}_i$ of unit length can rotate freely on the unit sphere. We consider a nearest-neighbor DM interaction strength $|\mathbf{D}| = D$ and for symmetry reasons we assume DM vectors which both lie in the plane of the magnetic film and are perpendicular to the connection line between neighboring spins [34]. The values of J_{ij}, K_i, $\mathbf{e}_{K_i}$, μ, and $\mathbf{B}$ provide the exchange-energy parameter, the anisotropy energy parameter, the direction of the uniaxial anisotropy, the magnetic moment, and an external magnetic field. A detailed phase space of a magnetic film which can be described by a Hamiltonian of the type given in Eq. (1) with an isotropic environment can

*jhagemei@physnet.uni-hamburg.de

 ©2016 American Physical Society

be found elsewhere [5,17,18,35]. In a broad parameter range, a spin-spiral state with a fixed rotational sense is the ground state at low temperatures and zero external magnetic field. The application of a perpendicular external magnetic field can cause a transition from the spin-spiral state to a skyrmionic state at an intermediate field strength, and eventually the saturated ferromagnetic state is reached at a sufficiently large field.

For the following investigations, we used two-dimensional triangular lattices which are similar in structure to pseudomorphically grown monoatomic layers on a (111) surface of a fcc crystal, such as, for example, Fe on Ir(111). The behavior of multiple magnetic layers is mimicked by spatial modulations of the parameters of the anisotropy energy and exchange interaction. We consider periodic modulations along the crystallographic direction $[10\bar{1}]$ which is motivated by the areas with periodic reconstruction features in the double and triple atomic layers of Fe on Ir(111). Reconstruction lines which are aligned parallel with periodicities of 5.2 nm and 4–9 nm, respectively, were reported [28,29].

II. SKYRMIONS WITH SPATIALLY MODULATED EXCHANGE-ENERGY PARAMETERS

Similar to previous investigations [36,37], effective nearest-neighbor exchange interaction parameters J_{ij} are introduced. However, we go beyond the earlier model and modulate the strength of the exchange coupling, not only as a function of the orientation of the respective bond, but as a generalization also of the position in the lattice according to the following description:

$$J_{ij}^2(\mathbf{r}_i,\mathbf{r}_j) = \left(j_{\mathrm{M}}^2 \frac{|\mathbf{e}\cdot\mathbf{r}_{ij}|^2}{a^2} + j_{\mathrm{m}}^2 \frac{|\mathbf{e}\times\mathbf{r}_{ij}|^2}{a^2} \right), \tag{2}$$

$$\mathbf{e}^T(\alpha) = [\cos(\alpha), \sin(\alpha), 0], \tag{3}$$

$$\alpha = \alpha_{\max} \sin\left(\frac{2\pi}{\lambda} \left[\frac{1}{2}(\mathbf{r}_i + \mathbf{r}_j)\cdot \mathbf{e}_{[10\bar{1}]} \right] \right), \tag{4}$$

with a being the lattice constant. Equation (2) is equivalent to the parametrization of an ellipse with the semimajor axis j_{M} and semiminor axis j_{m} in the case of $j_{\mathrm{M}} > j_{\mathrm{m}}$. The ellipse lies within the plane of the magnetic film, and the direction of the major axis $\mathbf{e}$ is locally rotated by the angle α with respect to the $[10\bar{1}]$ direction. $\boldsymbol{r}_{ij}$ is the vector connecting lattice sites i and j. The choice of unequal parameters j_{M} and j_{m} provides an anisotropic environment with an exchange interaction strength which then depends on the crystallographic orientation of a bond. The angle $\alpha_{\max}$ and the period λ can be used to create a periodic modulation of the anisotropic environment of the exchange interaction along the crystallographic direction $[10\bar{1}]$.

Figure 1(a) shows the perpendicular component of the magnetization of a spin-spiral state for the modulation period $\lambda = 20\,a$ and modulation angle $\alpha_{\max} = 29°$. The interaction strengths are $j_{\mathrm{m}}/j_{\mathrm{M}} = 0.5$ and $j_{\mathrm{m}}/D = 1.6$, and the anisotropy is $K = 0$. The temperature of the system was decreased from $k_{\mathrm{B}}T/D = 1.7$ to $k_{\mathrm{B}}T/D = 8.6 \times 10^{-3}$ using 20 temperature steps with $\sim 10^5$ Monte Carlo steps each, ensuring that the global energy minimum is reached. We used a single-spin

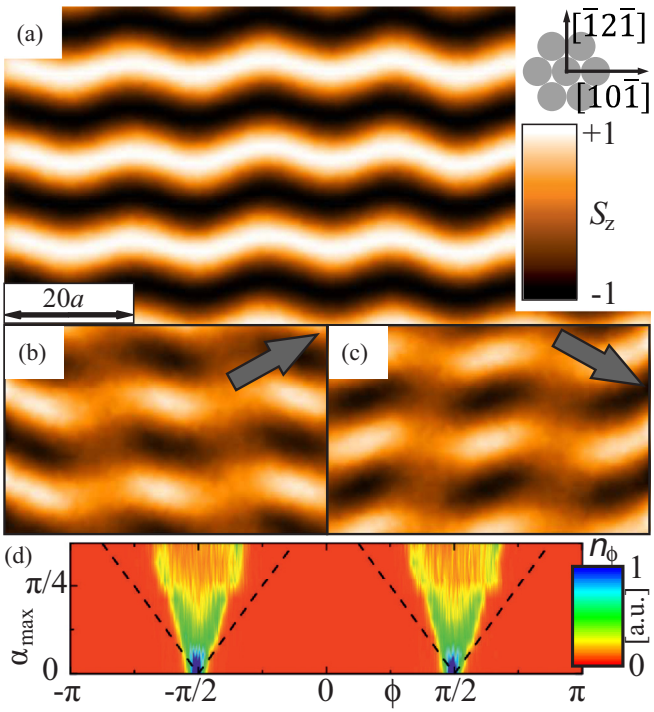

FIG. 1. Spin-spiral state with zigzag-shaped wave fronts on a triangular lattice with periodic boundary conditions in the $[\bar{1}2\bar{1}]$ direction. The color maps give a linear scheme of the projection of the magnetization onto a given direction which is perpendicular to the plane in (a) and parallel to the gray arrows in (b) and (c). (d) The frequency of the azimuthal angle ϕ with respect to the $[10\bar{1}]$ direction.

update mechanism based on the Metropolis algorithm [38]. The resulting spin spirals have a wavelength of approximately $14\,a$. The wave fronts are on average aligned parallel to the $[10\bar{1}]$ direction, and the periodicity of their zigzag pattern is in agreement with the modulation period of the exchange energy. Part of the spin contrast vanishes [Figs. 1(b) and 1(c)] when calculating the projection of the in-plane component of the magnetization onto the directions which enclose an angle of $\pm\alpha_{\max} = \pm 29°$ with the $[10\bar{1}]$ direction. This finding can be verified by the investigation of the incidence n_ϕ of the spins' azimuthal angles ϕ with respect to the $[10\bar{1}]$ direction, which is shown in Fig. 1(d). With a vanishing modulation amplitude $\alpha_{\max} = 0$, the spins are aligned in the plane given by the system's normal vector and the $[\bar{1}2\bar{1}]$ direction. An increase of the modulation amplitude $\alpha_{\max}$ causes the single peaks at $\pm 0.5\,\pi$ to split into double peaks with a distance of approximately $\alpha_{\max}$. Consequently, the spins are predominantly perpendicular to the local spin-spiral wave fronts, as expected for cycloidal spin spirals [1]. The present model seems to capture the main features of the spin-spiral states which have been observed experimentally in the double and triple atomic layers of Fe on Ir(111) [28,29].

However, it is more intriguing to explore the influence of the modulation of the exchange energy onto the Skyrmion state. Figures 2(a)–2(f) show the magnetic ground states which are obtained when the temperature of the system is reduced with applied constant magnetic fields. Except for the magnetic field, the energy parameters are chosen to be the same as before with

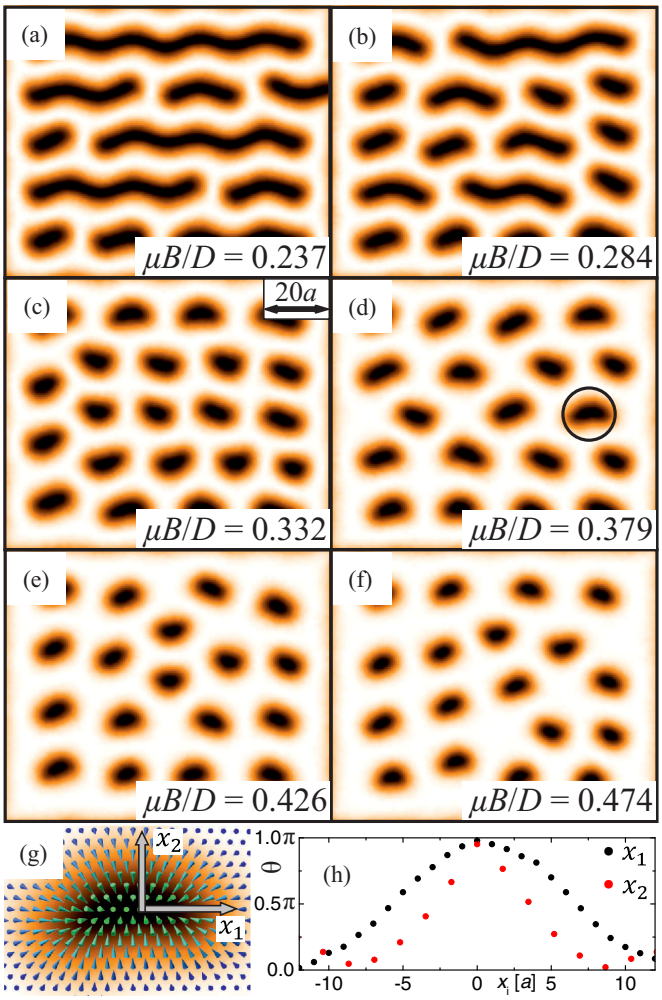

FIG. 2. (a)–(f) Color maps of the perpendicular component of the magnetization for the states which are obtained after cooling processes with different external magnetic fields using a modulated exchange-energy environment. (g) Spin texture of the magnetic object marked in (d). (h) Profiles of the polar angle for the magnetic texture in (g).

$\alpha_{\max} = 29°$. The spin spirals break up at the magnetic field $\mu B/D = 0.237$, and elongated zigzag structures are created which eventually shrink at magnetic field strengths larger than $\mu B/D = 0.284$. No individual magnetic objects are observed for fields larger than $\mu B/D = 0.62$. The magnetic objects possess a unique rotational sense and yield a nonvanishing topological charge Q which is usually defined via

$$Q = \frac{1}{4\pi}\int_A \mathbf{m}\cdot\left(\frac{\partial \mathbf{m}}{\partial x}\times\frac{\partial \mathbf{m}}{\partial y}\right)dxdy \qquad (5)$$

as an integral over the magnetic surface A whose local direction of magnetization is described by the continuous field $\mathbf{m}$. For the present investigations, an adoption of the formula for discrete systems is used [39,40]. Furthermore, the magnetic objects are nonaxisymmetric, as investigated exemplarily for the marked spin texture in Fig. 2(d). Figures 2(g) and 2(h) show the atomic spin configuration and the corresponding line profiles of the spins' polar angles. The profiles of the polar angle of the local magnetization direction clearly show an elongation of the structure into the $[10\bar{1}]$ direction compared to the $[\bar{1}2\bar{1}]$ direction.

III. SKYRMIONS WITH SPATIALLY MODULATED MAGNETOCRYSTALLINE ANISOTROPY

So far, we have focused on the effects of a spatial modulation of the exchange-energy parameter in skyrmionic materials and neglected the anisotropy energy. However, from previous studies it is known that the anisotropy energy can in principle vary locally in thin magnetic films [41]. In the following, we investigate the effects of a spatial modulation of the anisotropy energy in combination with an isotropic environment of the exchange and DM interaction. We introduce stripelike regions with an easy in-plane axis parallel to the $[\bar{1}2\bar{1}]$ direction and easy in-plane axis parallel to the $[10\bar{1}]$ direction of the widths $dl_1 = 18\,a$ and $dl_2 = 2\,a$, which are periodically repeated along the $[10\bar{1}]$ direction with a periodicity of $20\,a$. In Fig. 3(a), a sketch of the atomic lattice is given, indicating the anisotropy axis for each lattice site. The same anisotropy energy constant of $K/D = 0.6$ is assumed for the two regions and $J/D = 2.1$ is chosen. Figures 3(b)–3(d) show the magnetic ground states for different magnetic fields after the reduction of the temperature in the same fashion as before. The spin-spiral period at zero magnetic field is approximately $15.8\,a$ and the wave fronts are aligned in parallel to the $[10\bar{1}]$ direction. With an applied magnetic field of $\mu B/D = 0.52$, an ordered state of elongated magnetic objects is formed. Their centers lie in the middle of the regions that possess an anisotropy axis parallel to the $[\bar{1}2\bar{1}]$ direction, and their elongation into the $[10\bar{1}]$ direction is determined by the areas in which the anisotropy axis is parallel to the $[10\bar{1}]$ direction. This finding is verified exemplarily for a single magnetic object which is highlighted in Fig. 3(c). Figure 3(e) shows

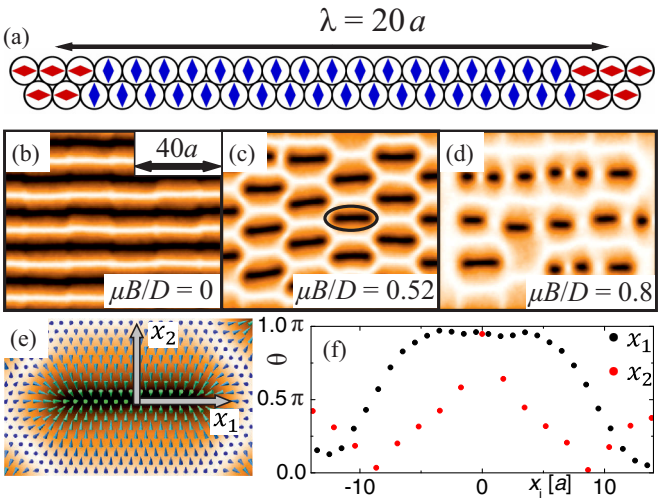

FIG. 3. (a) Sketch of the atomic lattice in the top view indicating regions of easy in-plane anisotropy axes parallel to the $[10\bar{1}]$ (red) and $[\bar{1}2\bar{1}]$ (blue) direction. (b)–(d) Color maps of the perpendicular component of the magnetization of the states obtained after cooling processes with different external magnetic fields. (e) Spin configuration of a Skyrmion marked in (c). (f) Profiles of the polar angle through the magnetic texture shown in (e).

the corresponding spin configuration, and Fig. 3(f) displays the profiles of the polar angle of the magnetization along two perpendicular crystallographic axes. One can clearly discern a lateral size of the magnetic object parallel to the $[10\bar{1}]$ direction of about $20\,a$. In other words, the modulation of the anisotropy energy aligns the magnetic objects on tracks along the $[\bar{1}2\bar{1}]$ direction. For magnetic fields larger than $\mu B/D \approx 0.7$, a part of the magnetic objects splits into two smaller parts and eventually the ferromagnetic state is reached at fields larger than $\mu B/D \approx 0.9$.

IV. SKYRMIONS ON TRACKS

In the following, we want to gain insight into the formation of linearly aligned skyrmionic structures along a track by a spatial modulation of the energy parameters in a two-dimensional model system. For this purpose, we combine the effects of the modulation of the exchange and anisotropy energy with an isotropic environment of the DM interaction on the magnetic ground state of skyrmionic systems. The parameters for the exchange and DM interaction are chosen as in the simulations for Figs. 1 and 2. Additionally, we assume a spatial modulation of an easy in-plane anisotropy axis with the energy $K/D = 0.6$ similar to simulations for Fig. 3 but partly adopt the anisotropy axes to follow the modulation of the exchange interaction as indicated in Fig. 4(a), i.e., they are locally parallel to the minor axis of the exchange modulation scheme. For two magnetic fields, the magnetic ground states at low temperatures are shown in Figs. 4(b) and 4(c). One observes ordered bent noncollinear spin states with a nonvanishing topological charge at the magnetic field $\mu B/D = 0.52$ which appear at $\mu B/D \approx 0.71$ with a larger spatial separation and are not observed for $\mu B/D \gtrsim 0.85$. As before, the magnetic objects are aligned along tracks parallel to the $[\bar{1}2\bar{1}]$ direction. However, the magnetic objects of neighboring tracks influence each other in the current status in such a way that they could not be moved independently from each other parallel to the $[\bar{1}2\bar{1}]$ direction. We exclude every second track by locally substituting the easy in-plane axis by an easy out-of-plane anisotropy axis with the energy $K/D = 0.6$. The resulting magnetic equilibrium Skyrmion-like patterns are confined to spatially separated tracks parallel to the $[\bar{1}2\bar{1}]$ direction [Figs. 4(d) and 4(e)] (see Appendix A also). In real systems, this creation of tracks could be achieved by nanostructuring of the surface. We take a closer look at the spatial distribution of the topological charge and the energy densities for the obtained magnetic objects. The largest contributions to the topological charge arise at their ends, and a contribution of opposite sign is acquired near the bend, as can be observed in Fig. 4(f). The sum over the local contributions to the topological charge provides $Q = 1$ for each magnetic object. The exchange energy is large where the DM energy is small, as in the region where the magnetic moments have a perpendicular component opposite to the external magnetic field (Fig. 5). The anisotropy energy is small in regions where the spins of the magnetic objects lie predominantly within the magnetic layer, which is expected when considering the choice of the directions for easy anisotropy axes, as shown in the bottom of the individual images in Fig. 5 or in Fig. 4(a). Especially, the anisotropy energy is small at the ends of the elongated objects,

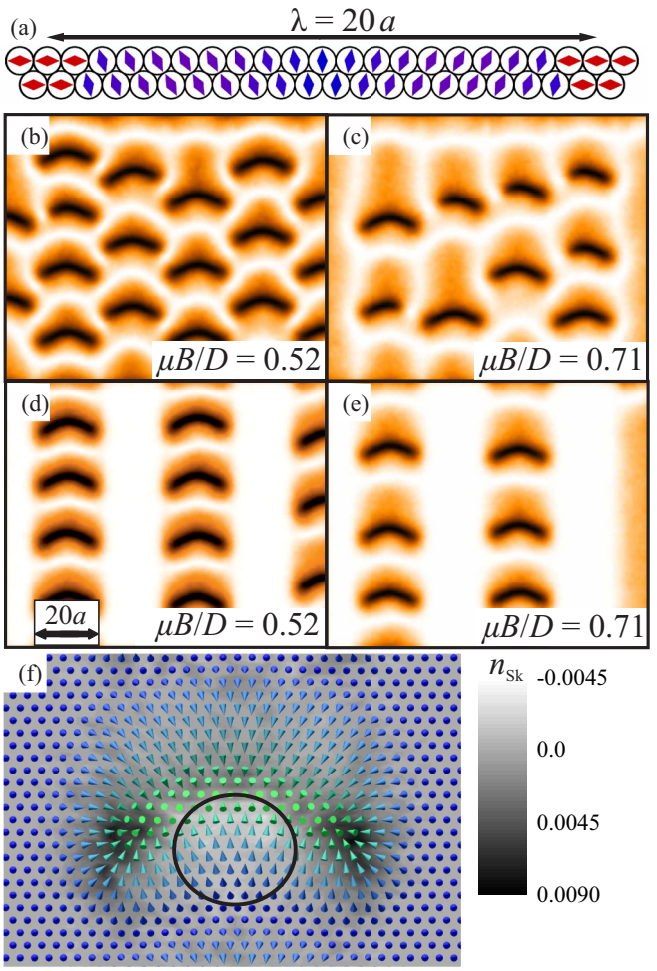

FIG. 4. (a) Sketch of the atomic lattice in the top view indicating the spatial modulation of the direction of the easy anisotropy axis. (b, c) Color maps of the perpendicular component of the magnetization of states obtained after cooling processes with different applied magnetic fields. The spatially modulated anisotropy energy is combined with the anisotropic environment of the exchange interaction used in Figs. 1 and 2 and an isotropic environment of the DM interaction. (d, e) Formation of Skyrmion tracks by a spatial modulation of local magnetic anisotropy as explained in the text. (f) Spin structure and local Skyrmion density for a magnetic object shown in (d). Within the marked area, topological charge of negative sign is acquired.

as indicated by the red arrows. The ends coincide with the narrow regions where the anisotropy axis is oriented parallel to the $[10\bar{1}]$ direction (see Fig. 5). This confines the Skyrmionic structure spatially in the $[10\bar{1}]$ direction and additionally prevents them from decreasing their size in the $[10\bar{1}]$ direction due to their pinning effect. In between these regions, the easy anisotropy axis is locally parallel to the minor axis of the exchange-energy modulation scheme, which suppresses, in combination with the direction-dependent exchange-energy parameter, a splitting of the magnetic objects and stabilizes them over a relatively large magnetic field range. Hence, both the exchange interaction and the anisotropy energy are responsible for the stabilization of the elongated skyrmionic structures.

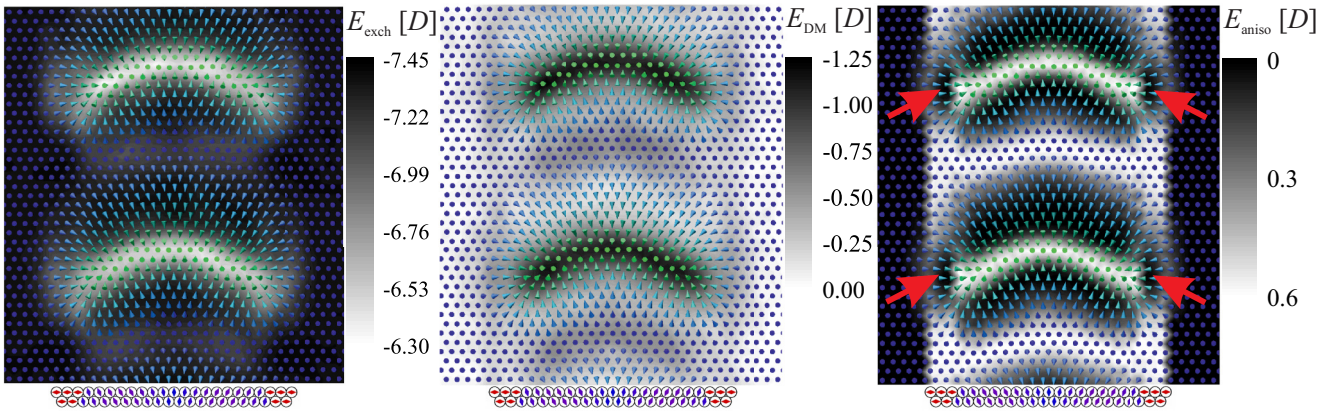

FIG. 5. The energy densities of the exchange interaction E_{exch}, the DM interaction E_{DM}, and the anisotropy energy E_{aniso} for two Skyrmions shown in Fig. 4(d). In the bottom, the local orientations of the easy anisotropy axes are indicated [same as in Fig. 4(a)]. The red arrows indicate the regions in which the in-plane part of the magnetic objects pin to the edges of the magnetic track due to the anisotropy energy.

V. CONCLUSION

To summarize, we have shown possible influences of spatial modulations of the exchange interaction and anisotropy energy onto the formation of noncollinear spin states in combination with an isotropic environment of a DM interaction and obtained deformed skyrmionic objects. Initially, magnetic Skyrmions were introduced as axisymmetric objects with a nonvanishing topological charge that forms in the presence of DM interaction, the exchange interaction, and the magnetocrystalline anisotropy. Since the magnetic objects that we have found possess the topological charge $Q = 1$ and have equilibrium sizes $\lesssim 10$ nm, they exhibit, indeed, the main characteristics of Skyrmions.

ACKNOWLEDGMENTS

We thank Pin-Jui Hsu, Niklas Romming, Lorenz Schmidt, Aurore Finco, André Kubetzka, and Kirsten von Bergmann for discussions. Financial support from the Deutsche Forschungsgemeinschaft in the framework of the SFB668 as well as from the European Union (FET-Open MagicSky Grant No. 665095) is gratefully acknowledged.

APPENDIX: SKYRMION MANIPULATION WITH A MAGNETIC TIP ALONG A TRACK

In the following, we discuss the mobility of the Skyrmions in the system presented in Figs. 4(d) and 4(e) of the main manuscript. The Skyrmions are aligned along tracks due to energy barriers resulting from a spatial modulation of the anisotropy landscape. However, this confinement is restricted to the $[10\bar{1}]$ direction, while the Skyrmions can be moved by a driving force along the $[\bar{1}2\bar{1}]$ direction which we will demonstrate in the following.

As a driving mechanism, we consider the spin-polarized current from a magnetic tip of scanning tunneling microscope. The influence can be described by an additional term [42] H_{T} in the Hamiltonian for Monte Carlo calculations:

$$H_{\mathrm{T}} = -g \sum_i \mathbf{T}_{\mathrm{i}} \cdot \mathbf{S}_{\mathrm{i}}, \tag{A1}$$

$$\mathbf{T}_{\mathrm{i}} = -I_0 \exp(-2\kappa \sqrt{(x_i - x_{\mathrm{tip}})^2 + (y_i - y_{\mathrm{tip}})^2 + h^2}) P \mathbf{m}_{\mathrm{tip}}. \tag{A2}$$

Therein, g is a coupling constant and T_{i} takes the spin-polarized current into account. P is the tip polarization, $\mathbf{m}_{\mathrm{tip}}$ a unity vector parallel to the magnetization direction of the tip, κ the inverse decay length in vacuum, $\mathbf{r}_{\mathrm{i}} = (x_i, y_i, 0)$ and $\mathbf{r}_{\mathrm{tip}} = (x_{\mathrm{tip}}, y_{\mathrm{tip}}, h)$ the positions of the lattice sites, and the tip and I_0 the spin-polarized current. We use typical values for the decay length $\kappa = 3\text{Å}^{-1}$ and the current $I_0 = 10^5 \frac{\mu_s}{\gamma D}$ [42]. The tip velocity is set to 1.5×10^{-5} lattice constants per Monte Carlo step. The position of the tip is updated in intervals of 5000 Monte Carlo steps. The magnetization direction of the tip is chosen parallel to the Skyrmion center, and $g = 1$ and $h = 1a$ with a being the lattice constant. We find that the tip is able to move the Skyrmions of Fig. 4(d) of the main text along the track at the temperature $k_{\mathrm{B}}T/D = 0.086$ as presented in the supplemental video [43]. The tip is positioned above a Skyrmion, and when the tip is moved along the track, it moves the Skyrmion along. This causes the other Skyrmions to move as well. We imposed periodic boundary conditions in the direction of the tracks. Therefore, the Skyrmions that leave the sample at one side reappear at the opposite side of the sample.

[1] A. Bogdanov and A. Hubert, J. Magn. Magn. Mater. **138**, 255 (1994).

[2] A. Bogdanov and A. Hubert, Phys. Status Solidi B **186**, 527 (1994).

[3] C. Pappas, E. Lelièvre-Berna, P. Falus, P. M. Bentley, E. Moskvin, S. Grigoriev, P. Fouquet, and B. Farago, Phys. Rev. Lett. **102**, 197202 (2009).

[4] S. Mühlbauer, B. Binz, F. Jonietz, C. Pfleiderer, A. Rosch, A. Neubauer, R. Georgii, and P. Böni, Science **323**, 915 (2009).

[5] X. Yu, Y. Onose, N. Kanazawa, J. Park, J. Han, Y. Matsui, N. Nagaosa, and Y. Tokura, Nature (London) **465**, 901 (2010).

[6] X. Z. Yu, N. Kanazawa, Y. Onose, K. Kimoto, W. Z. Zhang, S. Ishiwata, Y. Matsui, and Y. Tokura, Nat. Mater. **10**, 106 (2011).

[7] A. Tonomura, X. Yu, K. Yanagisawa, T. Matsuda, Y. Onose, N. Kanazawa, H. S. Park, and Y. Tokura, Nano Lett. **12**, 1673 (2012).

[8] S. Seki, X. Z. Yu, S. Ishiwata, and Y. Tokura, Science **336**, 198 (2012).

[9] E. Moskvin, S. Grigoriev, V. Dyadkin, H. Eckerlebe, M. Baenitz, M. Schmidt, and H. Wilhelm, Phys. Rev. Lett. **110**, 077207 (2013).

[10] S. Heinze, K. von Bergmann, M. Menzel, J. Brede, A. Kubetzka, R. Wiesendanger, G. Bihlmayer, and S. Blügel, Nat. Phys. **7**, 713 (2011).

[11] N. Romming, C. Hanneken, M. Menzel, J. E. Bickel, B. Wolter, K. von Bergmann, A. Kubetzka, and R. Wiesendanger, Science **341**, 636 (2013).

[12] N. Romming, A. Kubetzka, C. Hanneken, K. von Bergmann, and R. Wiesendanger, Phys. Rev. Lett. **114**, 177203 (2015).

[13] N. S. Kiselev, A. Bogdanov, R. Schäfer, and U. K. Rößler, J. Phys. D: Appl. Phys. **44**, 392001 (2011).

[14] A. Fert, V. Cros, and J. Sampaio, Nat. Nanotechnol. **8**, 152 (2013).

[15] I. Dzyaloshinskii, J. Phys. Chem. Solids **4**, 241 (1958).

[16] T. Moriya, Phys. Rev. **120**, 91 (1960).

[17] S. Banerjee, J. Rowland, O. Erten, and M. Randeria, Phys. Rev. X **4**, 031045 (2014).

[18] R. Keesman, A. O. Leonov, P. van Dieten, S. Buhrandt, G. T. Barkema, L. Fritz, and R. A. Duine, Phys. Rev. B **92**, 134405 (2015).

[19] K. Shibata, J. Iwasaki, N. Kanazawa, S. Aizawa, T. Tanigaki, M. Shirai, T. Nakajima, M. Kubota, M. Kawasaki, H. Park *et al.*, Nat. Nanotechnol. **10**, 589 (2015).

[20] M. Heide, G. Bihlmayer, and S. Blügel, Phys. Rev. B **78**, 140403 (2008).

[21] L. Bergqvist, A. Taroni, A. Bergman, C. Etz, and O. Eriksson, Phys. Rev. B **87**, 144401 (2013).

[22] B. Zimmermann, M. Heide, G. Bihlmayer, and S. Blügel, Phys. Rev. B **90**, 115427 (2014).

[23] L. Rózsa, L. Udvardi, L. Szunyogh, and I. A. Szabo, Phys. Rev. B **91**, 144424 (2015).

[24] B. Dupé, M. Hoffmann, C. Paillard, and S. Heinze, Nat. Commun. **5**, 4030 (2014).

[25] B. Dupé, G. Bihlmayer, M. Böttcher, S. Blügel, and S. Heinze, Nat. Commun. **7**, 11779 (2016).

[26] S. Woo, K. Litzius, B. Krüger, M. Im, L. Caretta, K. Richter, M. Mann, A. Krone, R. Reeve, M. Weigand *et al.*, Nat. Mater. **15**, 501 (2016).

[27] C. Moreau-Luchaire, C. Moutafis, N. Reyren, J. Sampaio, C. Vaz, N. Van Horne, K. Bouzehouane, K. Garcia, C. Deranlot, P. Warnicke *et al.*, Nat. Nanotechnol. **11**, 444 (2016).

[28] P. J. Hsu, A. Finco, L. Schmidt, A. Kubetzka, K. von Bergmann, and R. Wiesendanger, Phys. Rev. Lett. **116**, 017201 (2016).

[29] P. J. Hsu, A. Kubetzka, A. Finco, N. Romming, K. von Bergmann, and R. Wiesendanger, arXiv:1601.02935.

[30] J. Iwasaki, M. Mochizuki, and N. Nagaosa, Nat. Nanotechnol. **8**, 742 (2013).

[31] Y. Zhou and M. Ezawa, Nat. Commun. **5**, 4652 (2014).

[32] I. Purnama, W. Gan, D. Wong, and W. Lew, Sci. Rep. **5**, 10620 (2015).

[33] E. Y. Vedmedenko, H. P. Oepen, and J. Kirschner, J. Magn. Magn. Mater. **256**, 237 (2003).

[34] A. Crépieux and C. Lacroix, J. Magn. Magn. Mater. **182**, 341 (1998).

[35] A. Siemens, Y. Zhang, J. Hagemeister, E. Vedmedenko, and R. Wiesendanger, New J. Phys. **18**, 045021 (2016).

[36] E. Y. Vedmedenko, A. Kubetzka, K. von Bergmann, O. Pietzsch, M. Bode, J. Kirschner, H. P. Oepen, and R. Wiesendanger, Phys. Rev. Lett. **92**, 077207 (2004).

[37] E. Y. Vedmedenko, K. von Bergmann, H. Oepen, and R. Wiesendanger, J. Magn. Magn. Mater. **290-291**, 746 (2005).

[38] M. E. J. Newman and G. T. Barkema, *Monte Carlo Methods in Statistical Physics* (Oxford University Press, Oxford, UK, 1999).

[39] B. Berg and M. Lüscher, Nucl. Phys. B **190**, 412 (1981).

[40] A. van Oosterom and J. Strackee, IEEE Trans. Biomed. Eng. **BME-30**, 125 (1983).

[41] F. Porrati, W. Wulfhekel, and J. Kirschner, J. Magn. Magn. Mater. **270**, 22 (2004).

[42] T. Stapelfeldt, R. Wieser, E. Y. Vedmedenko, and R. Wiesendanger, Phys. Rev. Lett. **107**, 027203 (2011).

[43] See Supplemental Material at http://link.aps.org/supplemental/10.1103/PhysRevB.94.104434 for a video of the lateral skyrmion movement induced by a spin-polarized electric current of a magnetic tip.